



Urea-related reactions and their active sites over Cu-SAPO-34: Formation of NH₃ and conversion of HNCO

Yue Ma^a, Xiaodong Wu^{a,*}, Junyu Zhang^b, Rui Ran^a, Duan Weng^{a,*}

^a The Key Laboratory of Advanced Materials of Ministry of Education, School of Materials Science and Engineering, Tsinghua University, Beijing 100084, China

^b School of Environment, Tsinghua University, Beijing 100084, China



ARTICLE INFO

Keywords:

Cu-SAPO-34
Urea-SCR
Isocyanic acid
Copper species
NH₄NO₃ deposition

ABSTRACT

Urea-SCR is an efficient method to reduce NO_x emission from diesel vehicles, but the active sites of Cu-SAPO-34 for urea-related reactions have not been well identified. In the present work, a series of Cu-SAPO-34 catalysts with different copper species were prepared and tested for urea thermolysis, urea hydrolysis and urea-SCR. Temperature-programmed experiments and in-situ diffuse reflectance infrared Fourier transform spectroscopy (in-situ DRIFTS) were used to determine isolated Cu²⁺ ions as the main active sites for these reactions. HNCO (isocyanic acid) and NH₃ are formed via urea thermolysis. HNCO is less active than NH₃ to interact with NO_x and most of HNCO is hydrolyzed to produce NH₃ in urea-SCR. In the presence of NO₂, the reactivity of HNCO as a reducing agent is promoted, but both HNCO-SCR and HNCO hydrolysis would be inhibited by the deposition of NH₄NO₃. These findings provide a foundation for improving deNO_x efficiency of Cu-SAPO-34 catalysts on diesel vehicles.

1. Introduction

Selective catalytic reduction (SCR) is an effective method to eliminate NO_x in oxygen-rich exhaust gas from diesel vehicles and power plants. NH₃ is usually employed as a reducing agent, namely NH₃-SCR. However, it is inconvenient and unsafe to store gaseous NH₃ or ammonium hydroxide on diesel vehicles. Instead, 32.5 wt.% urea solution has been widely used as an ammonia source. After sprayed into hot exhaust gas, water is first evaporated from the urea solution. Then the urea undergoes thermolysis to give equal mole of HNCO (isocyanic acid) and NH₃ (Reaction (1)). HNCO is further hydrolyzed over catalysts to produce another molecule of NH₃ and CO₂ (Reaction (2)). The overall reaction of urea hydrolysis is shown as Reaction (3). Then the NH₃ originated from these reactions participates in NH₃-SCR (Reaction (4)). HNCO can also polymerize or interact with residual urea to produce biuret, CyA (cyanuric acid) and other solid deposits. These deposits can be decomposed or hydrolyzed to produce NH₃, HNCO and CO₂ at higher temperatures [1–7].



As the ammonia sources are different between urea-SCR in diesel vehicles and NH₃-SCR in laboratory study and stationary sources, catalysts may show different behaviors in these conditions. In real exhaust pipes of diesel vehicles, the residue time of urea is less than one second before reaching SCR catalysts, during which urea and HNCO cannot be completely decomposed and hydrolyzed [8,9]. Insufficient NH₃ supply may lead to decreased NO_x conversion [8,10,11] and increased slip of unreacted reducing agents [9,12]. The deposition of unreacted urea and solid by-products may also deactivate the catalysts [13,14] and clog the urea nozzles and the exhaust pipes [9,15], leading to more serious problems on the deNO_x system.

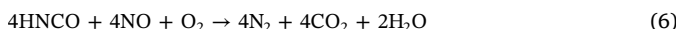
For urea-SCR on diesel vehicles, Cu-exchanged small pore zeolites are advanced catalysts, showing higher hydrothermal stability than other zeolite-based catalysts and vanadium-based catalysts supported on anatase [16–20]. However, it has been reported that zeolite-based catalysts have inferior activities for urea thermolysis and hydrolysis compared with anatase [21,22], making the insufficient NH₃ supply more troublesome. The catalytic activities, active sites, active intermediates, by-products and reaction kinetics of urea-related reactions over anatase and anatase-supported catalysts have been studied in detail since the last two decades [4,12,15,23–32]. Only limited research has been reported on urea thermolysis and hydrolysis over large- and medium-pore zeolite-based catalysts such as Fe-BEA, Cu-ZSM-5 and Fe-ZSM-5 [14,33–36], and so far there has been no report on the behaviors

* Corresponding authors.

E-mail addresses: wuxiaodong@tsinghua.edu.cn (X. Wu), duanweng@tsinghua.edu.cn (D. Weng).

of urea over small-pore silicoaluminophosphate, SAPO-34 and its Cu-loaded form, Cu-SAPO-34.

Because the SCR catalysts may suffer from insufficient supply of NH₃, it is meaningful to investigate whether HNCO can directly participate in SCR as a reducing agent, *i.e.*, HNCO-SCR in Reactions (5) and (6). If Reaction (5) takes place, one mole of HNCO will reduce 1.5 mol of NO, which has been observed in engine test over vanadium-based SCR catalysts [4]. Alternatively, the reaction of HNCO and NO can show a stoichiometric ratio of 1:1 with the participation of O₂ (Reaction (6)) [36]. Most recently, Seneque et al. [10] have reported a different reaction pathway of HNCO-SCR in fast SCR condition (NO:NO₂ = 1:1 in inlet) over a zirconia-based catalyst (Reaction (7)), similar to fast SCR reaction between NH₃ and NO_x (Reaction (8)). They also observed the reaction between HNCO and NO₂, which gives a quite complicated stoichiometry [8,10]. However, HNCO-SCR catalyzed by metal-exchanged zeolites, especially by Cu-SAPO-34 has not been reported yet.



To shed light on these unknown aspects, we prepared a series of Cu-SAPO-34 catalysts with different Cu loadings and dispersions in the present work. The urea thermolysis, hydrolysis and SCR reactions on the urea-loaded samples were studied by temperature-programmed experiments and in-situ diffuse reflectance infrared Fourier transform spectroscopy (in-situ DRIFTS). These experiments gave elementary information on the active sites of urea-related reactions over Cu-SAPO-34 and clarified the role of HNCO in urea-SCR, which contributed to overcoming the problem of possible reductant insufficiency in urea-SCR over Cu-SAPO-34 catalysts.

2. Experimental

2.1. Catalyst preparation

A commercial SAPO-34 zeolite (Nankai Catalyst, China) was used as the parent material. Cu²⁺ ions were loaded by a solution ion-exchange method. The zeolite was first ion-exchanged with a NH₄NO₃ solution to obtain the NH₄⁺-form of SAPO-34. Then, the NH₄-SAPO-34 powders were ion-exchanged with Cu²⁺ ions in a 0.1 mol/L Cu(CH₃COO)₂ solution at 70 °C. The ion-exchange time was adjusted to obtain Cu-SAPO-34 catalysts with approximately 1 wt.% and 2 wt.% Cu loadings, denoted as 1Cu-SAPO-34 and 2Cu-SAPO-34, respectively. Besides, two other samples with 1 wt.% Cu loading were prepared for reference. The sample with Cu_xO_y clusters as the dominant copper species was prepared via an impregnation method [37], except that the calcination time was shortened to 2 h to avoid solid-state ion-exchange [38]. The obtained sample was denoted as 1Cu-SAPO-34-i. The mechanical mixture of commercial CuO (Sinopharm, China) and SAPO-34 powders by using a mortar for 10 min was denoted as 1CuO/SAPO-34-m. The information of the catalysts was summarized in Table 1.

Urea was loaded onto the catalysts by an incipient-wetness impregnation method. Briefly, an appropriate amount of urea (Sinopharm, China) was dissolved in deionized water and impregnated on the catalysts. Then the samples were dried under ambient condition for 48 h. The nominal urea loading was 10 wt.%. Commercial TiO₂ (anatase), ZrO₂, SiO₂ and cordierite were also impregnated with urea as reference samples. Additionally, some 2Cu-SAPO-34 powders were mechanically mixed with urea in a mortar to study the influence of loading methods on the behavior of urea.

Table 1
Brief information of the catalysts.

Catalysts	Preparation methods	Cu loading ^a (wt.%)	S _{BET} ^b (m ² /g)	V _{total} ^b (cm ³ /g)
SAPO-34	Commercial zeolite	—	637.5	0.290
1Cu-SAPO-34	Ion-exchange	1.11	603.1	0.271
2Cu-SAPO-34	Ion-exchange	2.15	580.8	0.277
1Cu-SAPO-34-i	Impregnation	1.20	596.1	0.250
1CuO/SAPO-34-m	Mechanical mixing	1.02	589.6	0.268

^a Determined by H₂-TPR (Fig. S1).

^b Determined by N₂ physisorption.

2.2. Characterization

The textural properties of the catalysts were determined by nitrogen isothermal physisorption on a JW-BK122F surface area and pore size analyzer (JWGB, China). The samples were degassed at 220 °C for 3 h before measurement.

The Cu loadings and Cu species on the catalysts were identified by hydrogen temperature-programmed reduction (H₂-TPR) on an AutoChem II 2920 chemisorption analyzer (Micromeritics, USA). The samples were pretreated in 10% O₂/He at 300 °C for 30 min, and then cooled to room temperature. H₂-TPR was performed in 10% H₂/Ar at a temperature ramp of 10 °C/min to 800 °C.

2.3. Temperature-programmed experiments

Temperature-programmed urea thermolysis on different catalysts was compared on a TGA/DSC 1 thermal analysis system (Mettler Toledo, Switzerland) in air flow from room temperature to 800 °C at a heating rate of 10 °C/min.

To further study the behaviors of urea on SAPO-34 and Cu-SAPO-34 catalysts under different conditions, urea thermolysis, hydrolysis and the reactions between urea and NO_x were tested on a fixed-bed reactor and the outlet gas was monitored by a MKS 2030 Fourier transform infrared (FT-IR) gas analyzer (MKS Instruments, USA). For each test, 50 mg urea-impregnated sample was mixed with 200 mg quartz sand using a spatula, and then loaded in the fixed-bed reactor. O₂, NO and NO₂ were diluted in N₂ to simulate different reaction conditions with a total flow rate of 500 mL/min. Water vapor was added into the gas flow by bubbling N₂ into deionized water when used. The concentration of gaseous H₂O was about 5%. All the pipes of the reactor were heated above 100 °C to avoid water condensation. The heating rate in these experiments was set as 10 °C/min. The concentrations of NH₃, HNCO, CO₂, NO, NO₂ and N₂O in the outlet gas were measured by the gas analyzer. HNCO conversion was calculated by Eq. (9), in which the moles of the products were integrated over the whole temperature range.

$$\text{HNCO conversion} = \left(1 - \frac{n(\text{HNCO})_{\text{out}}}{n(\text{HNCO})_{\text{out}} + n(\text{CO}_2)_{\text{out}}} \right) \times 100\% \quad (9)$$

2.4. In-situ DRIFTS

In-situ diffuse reflectance infrared Fourier transform spectroscopy (in-situ DRIFTS) experiments were performed on a Nicolet 6700 spectrometer (ThermoFisher, USA) with a PIKE reaction chamber. The reaction conditions were similar to those in the temperature-programmed experiments. Spectra were collected at a resolution of 4 cm⁻¹.

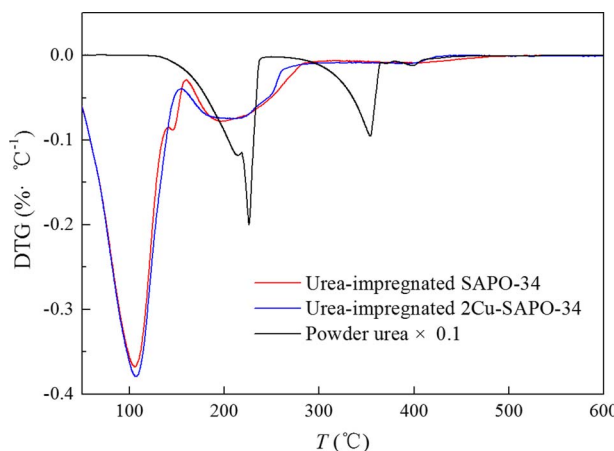


Fig. 1. DTG curves of urea and urea-impregnated SAPO-34 and 2Cu-SAPO-34 in air flow.

3. Results

3.1. Urea thermolysis over SAPO-34 and Cu-SAPO-34

3.1.1. DTG analysis

The non-catalytic and catalytic thermolysis of urea over SAPO-34 and 2Cu-SAPO-34 were analyzed by thermogravimetry and the results are shown in Fig. 1. Neat urea shows a typical two-stage thermolysis behavior, i.e., releasing NH₃ and HNCO (Reaction (1)) and forming by-products at temperatures below 250 °C and the further decomposition of by-products at temperatures higher than 250 °C [4,5,33,39]. Two mass loss peaks are also observed on urea-impregnated SAPO-34 and 2Cu-SAPO-34. The first peak below 150 °C is mainly attributed to evaporation of water introduced during the impregnation [5,21], and the second one at around 200 °C is attributed to urea thermolysis and NH₃ desorption. Urea thermolysis occurs at lower temperatures over 2Cu-SAPO-34 than over SAPO-34. The second stage of urea thermolysis disappears over the urea-impregnated samples, implying that the decomposition of the by-products is catalyzed by these materials, making two peaks merged into one [33]. DTG curves of urea thermolysis over cordierite, TiO₂ and ZrO₂ were also collected in Fig. S2. In accordance with the literatures, TiO₂ and ZrO₂ are highly active for urea thermolysis, which dramatically decrease the thermolysis temperature of urea, while 2Cu-SAPO-34 shows inferior urea thermolysis activity, similar to other zeolites such as ZSM-5 and Fe-Beta [21,22]. This result demonstrates that the deposition of urea and the corresponding by-products should be paid attention to when running urea-SCR over Cu-SAPO-34 catalysts.

3.1.2. Products of urea thermolysis

Because the DTG curves of urea thermolysis over the catalysts would be disturbed by H₂O and NH₃ desorption, the urea thermolysis experiments were also performed in a fixed bed reactor and the products were monitored by the FT-IR gas analyzer. Typical urea temperature-programmed thermolysis curves are shown in Fig. 2 and the other results are shown in Figs S3 and S4. The main products of urea thermolysis are NH₃ and HNCO, with a minor amount of CO₂, while the concentration of NO_x (including NO, NO₂ and N₂O) is less than 5 ppm. The corresponding thermolysis temperatures and product distributions are summarized in Table 2. It should be mentioned that in our laboratory study, urea was loaded by the incipient-wetness impregnation method, differing from gas phase deposition in realistic condition. However, by comparing with the mechanical mixture of urea and 2Cu-SAPO-34 (Fig. S5a), it can be inferred that different loading methods have little influence on the catalytic thermolysis behavior of urea over these catalysts. In addition, Bernhard et al. [15] have reported that loading urea by impregnation and conducting the experiments in a

fixed-bed reactor could simulate the actual condition in the exhaust pipes of diesel vehicles quite well.

As the release of NH₃ was delayed due to adsorption over SAPO-34 zeolite, the onset and finish temperatures of urea thermolysis could be defined by the temperatures that HNCO release started and finished, respectively. The HNCO release curves show a doublet shape or a main peak with several shoulders, suggesting that there are several stages in urea thermolysis over these catalysts [5]. The introduction of Cu species significantly reduces the onset temperature of urea thermolysis, and the finish temperature is also lowered. When the experiments were performed in N₂, some urea-related deposits are oxidized by Cu(II) species, leading to a small amount of CO₂ release with the maximal concentration of 20 ppm at temperatures higher than 250 °C. Little differences are found among these Cu-containing catalysts. However, in the presence of O₂, the catalysts with stronger oxidizing property (i.e., with higher Cu loadings or with more Cu_xO_y clusters) oxidize more HNCO to CO₂ at high temperatures and decrease the finish temperature of HNCO release. More than 50 ppm CO₂ is observed in the outlet gas at 350 °C in the presence of O₂ (Fig. 2d), even though only a little amount of HNCO is observed above this temperature in N₂ (Fig. 2c), indicating the oxidation of stable urea-related deposits over the copper-containing catalysts at high temperatures [39]. The oxidation process is also observed over pure SAPO-34 to a much lesser extent (Fig. 2b).

The detected molar ratios of NH₃ to HNCO over these samples are all close to 1, in accordance with Reaction (1) [2,5]. The CO₂ formation at temperatures below 150 °C arises from urea hydrolysis (Reactions (2) and (3)) by residual water adsorbed in the pores of the zeolite, leading to slightly higher yield of NH₃ than HNCO in N₂. When 5% O₂ is present as in the actual exhaust gas of diesel vehicles, the molar ratios of NH₃ to HNCO decrease, especially over 1Cu-SAPO-34-i, indicating that NH₃ is more susceptible than HNCO to being oxidized by O₂.

3.1.3. In-situ DRIFTS study

Urea thermolysis over different catalysts was also studied by in-situ DRIFTS and the spectra of HNCO-related species over SAPO-34 and 2Cu-SAPO-34 are shown in Fig. 3. Over pure SAPO-34, the band at 2264 cm⁻¹ and the shoulder at 2215 cm⁻¹ (Fig. 3a and b) can be attributed to NCO⁻ adsorbed on the framework Al and Si atoms of SAPO-34 with different chemical environments [27,34,35], as confirmed by the in-situ DRIFT spectra of urea thermolysis over SiO₂ and γ-Al₂O₃ (Fig. S6). These bands form at 150 °C, gradually increase in intensity at temperatures below 300 °C and then are weakened with increasing temperature and prolonging heating time, indicating the formation of HNCO species during urea thermolysis and its desorption/decomposition at higher temperatures [27]. At 500 °C, a board band occurs at 2179 cm⁻¹, which may be assigned to some stable HNCO-related species remaining on the zeolite. Over 2Cu-SAPO-34, M-NCO species are formed at lower temperatures and a strong band occurs at 2220 cm⁻¹ (Fig. 3c and d). This band is attributed to NCO⁻ adsorbed on Cu(II) species such as isolated Cu²⁺ ions and Cu_xO_y clusters [35], which is also observed over 1Cu-SAPO-34 and 1Cu-SAPO-34-i (Fig. S7). In the presence of 5% O₂, the bands over 2Cu-SAPO-34 decrease dramatically in intensity at temperatures higher than 300 °C (Fig. 3d), indicating that the NCO⁻ species are oxidized by O₂. This phenomenon is in good accordance with the generation of CO₂ as a product of the oxidation reaction detected in the fixed-bed reactor (Fig. 2d). Besides the NCO⁻ species, urea-related deposits such as biuret and CyA are also observed over the samples (Fig. S8), in accordance with the literatures [16,33].

3.2. Urea hydrolysis over SAPO-34 and Cu-SAPO-34

3.2.1. Urea conversion by hydrolysis

To improve deNO_x efficiency, HNCO generated from urea thermolysis should be further hydrolyzed via Reaction (2) to give another molecule of NH₃. To simulate urea hydrolysis in exhaust gas of diesel vehicles, 5% water vapor and 5% O₂ were added to the gas flow. The

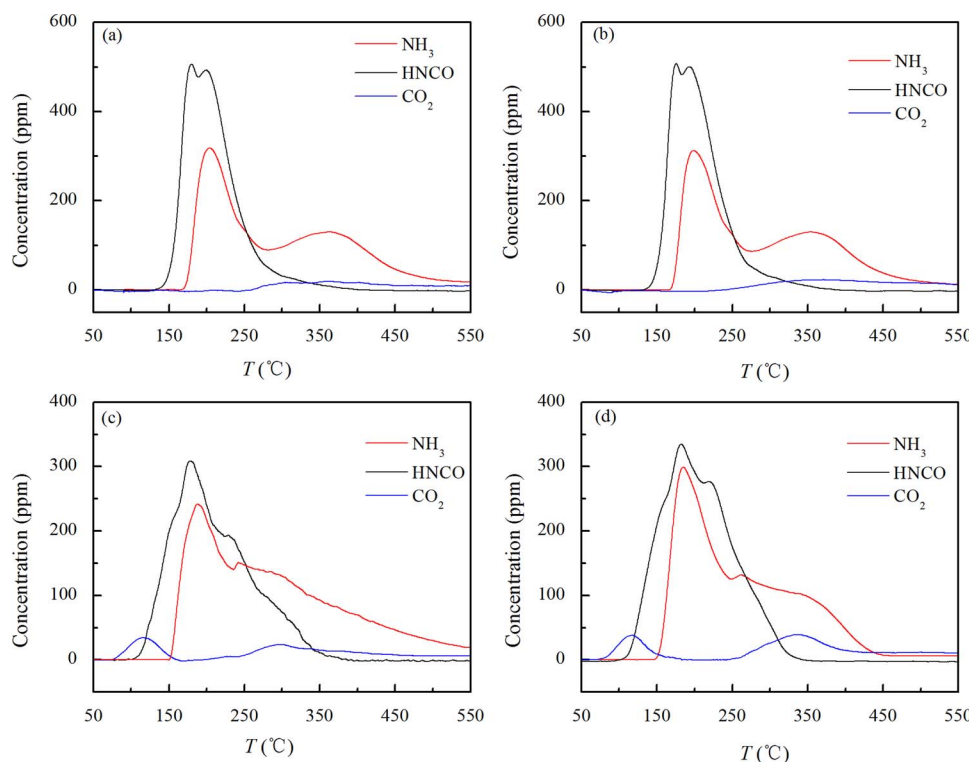


Fig. 2. Temperature-programmed thermolysis curves of urea over SAPO-34 in (a) N_2 and (b) 5% O_2/N_2 and over 2Cu-SAPO-34 in (c) N_2 and (d) 5% O_2/N_2 .

hydrolysis curves are shown in Fig. 4 and the results are summarized in Table 3. The detected molar ratios of N(–III) species (i.e., NH_3 and HNCO) to C-containing species (i.e., CO_2 and HNCO) in the outlet gas under different conditions are all close to that in urea molecule (namely, N: C = 2), suggesting that almost all urea and urea-related deposits are converted to NH_3 , HNCO and CO_2 , and NH_3 oxidation is not pronounced even in the oxygen-rich condition. Like the case in urea thermolysis, the loading methods do not affect the behavior of urea in catalytic hydrolysis, either (Fig. S5b).

It can be seen in Table 3 that SAPO-34 has inferior catalytic activity with only 62% HNCO conversion. The onset temperature of hydrolysis (represented by CO_2 release) over SAPO-34 is 120 °C, lower than that of urea thermolysis, indicating that H_2O can directly attack urea (Reaction (3)) or accelerate urea thermolysis (Reaction (1)) by acting as a proton shuttle [22]. Two HNCO release peaks centered at 170 and 240 °C can be found in Fig. 4a. The HNCO release peak at 170 °C suggests that HNCO hydrolysis is slower than urea thermolysis at low temperatures. With increasing temperature, HNCO hydrolysis is accelerated [22], resulting in a decrease in the concentration of slipped HNCO, along with a release peak of CO_2 at about 200 °C. This phenomenon was also observed over SiO_2 (Fig. S9a), as well as over an inert cordierite

monolith [21]. Although HNCO conversion increases monotonously with increasing temperature in HNCO hydrolysis tests using gaseous HNCO as the reactant [12,23,26,34], it is not the case when HNCO is produced locally via thermolysis of urea and its solid by-products. At temperatures higher than 220 °C, the slipped HNCO concentration increases again (Fig. 4a). This may be due to the decomposition of some solid by-products that are inert to interact with water vapor [4], or the decreased adsorption of HNCO and/or H_2O at high temperatures [12]. Even so, the finish temperature of HNCO release is significantly lower in urea hydrolysis test than in urea thermolysis test over SAPO-34, indicating that the presence of water vapor can impede the formation of solid by-products such as CyA and thus accelerate urea conversion [4,21,33].

Over Cu-containing catalysts, HNCO conversion is significantly improved, especially at 150–175 and 225–250 °C (Fig. 4b–d). The onset temperature of urea hydrolysis is reduced and an obvious shoulder peak of CO_2 release occurs at around 150 °C. By integrating the amount of CO_2 released below 160 °C and comparing it with the total amount of CO_2 released, it can be found that the proportion of CO_2 released at low temperatures increases from 0.07 over SAPO-34 to 0.27 over 2Cu-SAPO-34 (Table 3). These values demonstrate the catalytic activities of

Table 2
Results of urea thermolysis over the catalysts.

Catalysts	Reaction conditions	$NH_3/HNCO$ detected	Onset temperature of urea thermolysis ^a (°C)	Finish temperature of urea thermolysis ^b (°C)
SAPO-34	N_2	1.02	140	410
SAPO-34	5% O_2/N_2	1.00	139	406
1Cu-SAPO-34	N_2	1.12	103	396
1Cu-SAPO-34	5% O_2/N_2	1.07	104	375
2Cu-SAPO-34	N_2	1.14	102	396
2Cu-SAPO-34	5% O_2/N_2	1.07	101	367
1Cu-SAPO-34-i	N_2	1.14	102	395
1Cu-SAPO-34-i	5% O_2/N_2	0.94	103	367
1CuO/SAPO-34-m	N_2	0.96	137	406
1CuO/SAPO-34-m	5% O_2/N_2	0.94	136	386

^a The onset temperature of HNCO release.

^b The finish temperature of HNCO release.

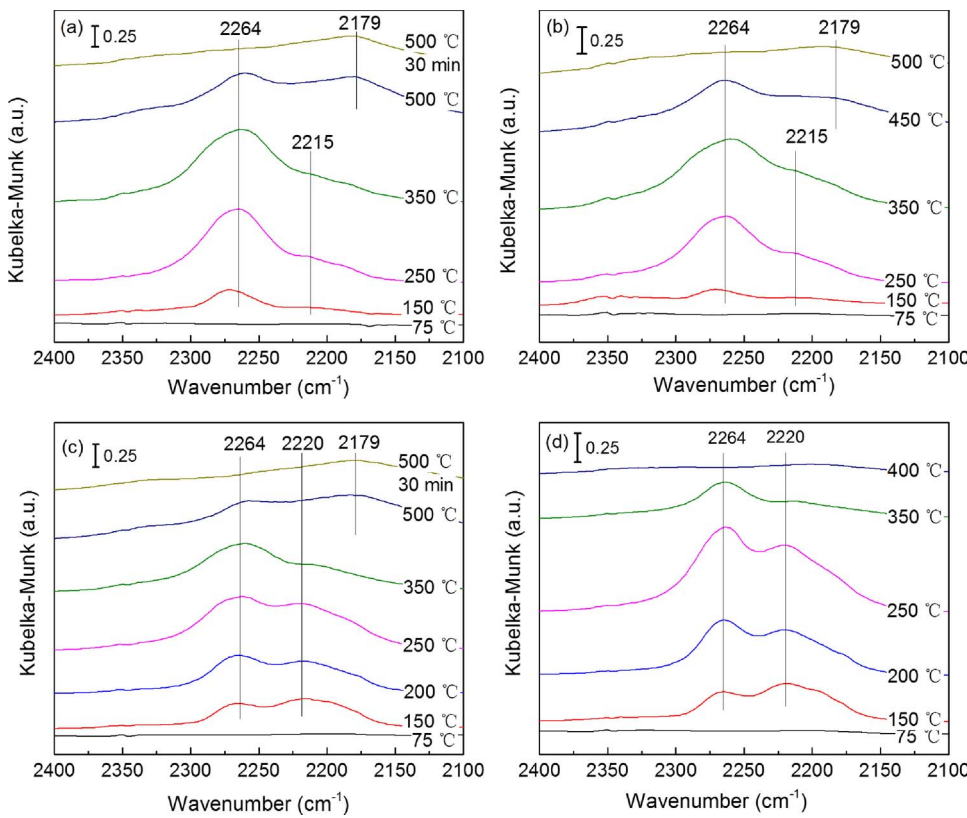


Fig. 3. In-situ DRIFT spectra of urea thermolysis over SAPO-34 in (a) N_2 and (b) 5% O_2/N_2 and over 2Cu-SAPO-34 in (c) N_2 and (d) 5% O_2/N_2 .

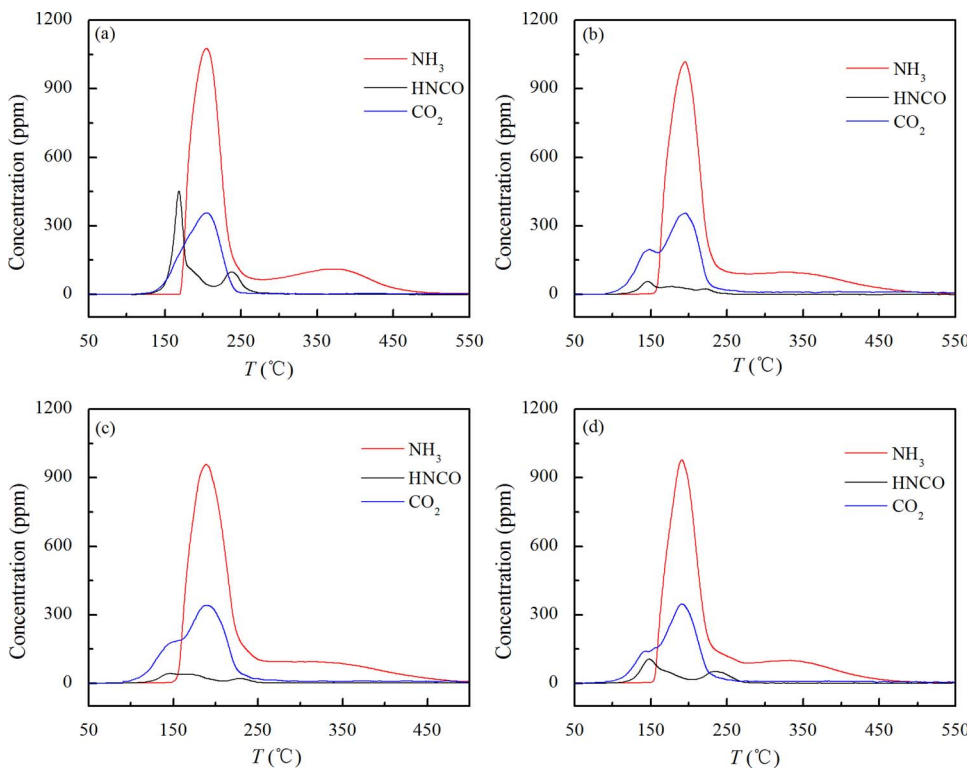


Fig. 4. Temperature-programmed hydrolysis curves of urea over (a) SAPO-34, (b) 1Cu-SAPO-34, (c) 2Cu-SAPO-34 and (d) 1Cu-SAPO-34-i in 5% $\text{H}_2\text{O}/5\% \text{O}_2/\text{N}_2$.

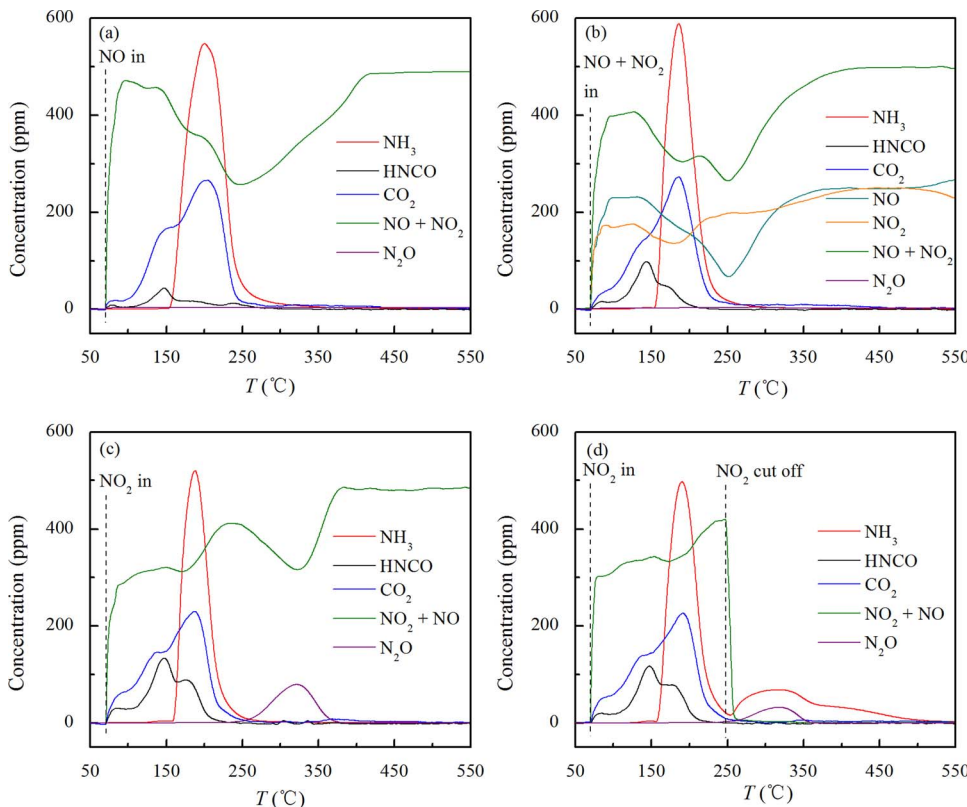
Cu species for low-temperature urea thermolysis and hydrolysis. The accumulation of solid deposits is inhibited, leading to a reduced HNCO slip at temperatures higher than 220 °C. The HNCO conversion increases slightly with increasing Cu loading, while the dispersion of Cu species has a more notable influence on HNCO conversion. The ion-exchanged 1Cu-SAPO-34 shows much higher activity than the

impregnated 1Cu-SAPO-34-i, while the mechanically mixed 1CuO/SAPO-34-m gives similar HNCO conversion to pure SAPO-34 (Fig. S4c and Table 3). Thus, isolated Cu^{2+} ions are identified as active sites for HNCO hydrolysis. Although 2Cu-SAPO-34 gives the highest HNCO conversion (88%) among these catalysts, its NH_3 formation efficiency is still much lower than TiO_2 , which converts almost all HNCO under the

Table 3

Results of urea hydrolysis over the catalysts.

Catalysts	HNCO conversion (%)	Onset temperature of hydrolysis ^a (°C)	Proportion of CO ₂ released below 160 °C ^b	Molar ratio of N(-III) to C in gaseous products ^c
SAPO-34	62	120	0.07	1.96
1Cu-SAPO-34	86	97	0.27	2.03
2Cu-SAPO-34	89	96	0.26	1.98
1Cu-SAPO-34-i	78	98	0.21	1.95
1CuO/SAPO-34-m	63	120	0.06	2.04

^a The onset temperature of CO₂ release.^b Calculated by dividing the amount of CO₂ that released below 160 °C by the total amount of CO₂.^c Calculated by $\frac{n(\text{NH}_3) + n(\text{HNCO})}{n(\text{CO}_2) + n(\text{HNCO})}$ detected in the outlet gas.**Fig. 5.** Temperature-programmed hydrolysis curves of urea over 2Cu-SAPO-34 in (a) 500 ppm NO/5% H₂O/5% O₂/N₂, (b) 250 ppm NO/250 ppm NO₂/5% H₂O/5% O₂/N₂, (c) and (d) 500 ppm NO₂/5% H₂O/5% O₂/N₂. The experiment of (d) repeated that of (c) except that NO₂ was cut off at 250 °C.

test condition (Fig. S9b).

3.2.2. Effect of NO_x on urea hydrolysis

To investigate the effect of NO_x on urea hydrolysis, NO and/or NO₂ were added to the gas flow. It can be seen in Figs. 5a, S10 and Table 4 that the presence of NO has little influence on urea hydrolysis and HNCO conversion, except that about 20 ppm of CO₂ was detected as soon as NO was cut in. This phenomenon indicates that HNCO can react with NO at low temperatures to a small extent. Meanwhile, the amount of released NH₃ is significantly reduced due to consumption in SCR reaction (Reaction (4)). The molar ratio of the consumed N(-III) species

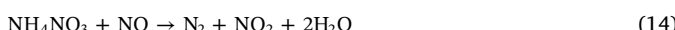
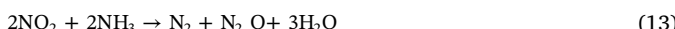
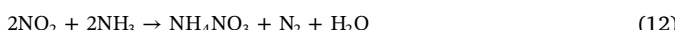
(i.e., NH₃ and HNCO) to the reduced NO_x was calculated by Eq. (10), in which the moles of the reactants and products were integrated over the whole temperature range. The ratios are close to 1 both on 2Cu-SAPO-34 (Fig. 5a) and 1Cu-SAPO-34 (Fig. S10b), excluding the possibility of Reaction (5) as the main reaction of HNCO-SCR in this case. Thus, the main reaction pathway of HNCO in Fig. 5a is being hydrolyzed to NH₃ and CO₂ (Reaction (2)), followed by NH₃-SCR (Reaction (4)).

Table 4Results of urea hydrolysis in the presence of NO_x over the catalysts.

Catalysts	Reaction conditions	HNCO conversion (%)	NO _x conversion (%)	$\frac{\text{Consumed N(-III)}}{\text{Reduced NO}_x}$
SAPO-34	500 ppm NO/5% H ₂ O/5% O ₂ /N ₂	62	< 5	—
1Cu-SAPO-34	500 ppm NO/5% H ₂ O/5% O ₂ /N ₂	85	14	1.06
2Cu-SAPO-34	500 ppm NO/5% H ₂ O/5% O ₂ /N ₂	90	15	1.02
2Cu-SAPO-34	250 ppm NO/250 ppm NO ₂ /5% H ₂ O/5% O ₂ /N ₂	82	17	1.03
2Cu-SAPO-34	500 ppm NO ₂ /5% H ₂ O/5% O ₂ /N ₂	71	15	1.04
2Cu-SAPO-34	500 ppm NO ₂ /5% H ₂ O/5% O ₂ /N ₂ , NO ₂ cutoff at 250 °C	73	—	—

$$\begin{aligned} \frac{\text{Consumed N(-III)}}{\text{Reduced NO}_x} (x = 1, 2) &= \frac{2 \times n(\text{Urea})_{\text{in}} - n(\text{NH}_3)_{\text{out}} - n(\text{HNCO})_{\text{out}}}{n(\text{NO})_{\text{in}} + n(\text{NO}_2)_{\text{in}} - n(\text{NO})_{\text{out}} - n(\text{NO}_2)_{\text{out}}} \\ &= \frac{2 \times [n(\text{CO}_2)_{\text{out}} + n(\text{HNCO})_{\text{out}}] - n(\text{NH}_3)_{\text{out}} - n(\text{HNCO})_{\text{out}}}{n(\text{NO})_{\text{in}} + n(\text{NO}_2)_{\text{in}} - n(\text{NO})_{\text{out}} - n(\text{NO}_2)_{\text{out}}} \\ &= \frac{2 \times n(\text{CO}_2)_{\text{out}} + n(\text{HNCO})_{\text{out}} - n(\text{NH}_3)_{\text{out}}}{n(\text{NO})_{\text{in}} + n(\text{NO}_2)_{\text{in}} - n(\text{NO})_{\text{out}} - n(\text{NO}_2)_{\text{out}}} \end{aligned} \quad (10)$$

In real diesel vehicle exhaust, part of NO is oxidized to NO_2 by an upstream DOC before reaching SCR catalysts, so NO_2 was also added to the simulated gas flow in the present work. It is obvious that urea hydrolysis is severely inhibited by NO_2 , both in $\text{NO}:\text{NO}_2 = 1:1$ (Fig. 5b) and NO_2 -only conditions (Fig. 5c). Piazzesi et al. [29] have reported that NO_2 inhibits HNCO hydrolysis over anatase via ammonium nitrate deposition. This may also be the case over Cu-SAPO-34, as suggested by a N_2O release peak at 250–375 °C (Fig. 5c). To give further proof on NH_4NO_3 formation, NO_2 was cut off at 250 °C in Fig. 5d. In this case, N_2O was still detected at 275–375 °C due to NH_4NO_3 decomposition (Reaction (11)), demonstrating that NH_4NO_3 had deposited at lower temperatures via Reaction (12) [40] or the reactions between NO_2 and urea/HNCO. The decomposition temperature of NH_4NO_3 over Cu-SAPO-34 (above 250 °C) is higher than those over other SCR catalysts such as cerium-based catalysts, ascribed to the strong acidity of SAPO-34 zeolite and the confinement effect caused by the small pore openings of SAPO-34 [41,42]. NH_3 slip is also detected after NO_2 cutoff, indicating that the N_2O release in Fig. 5c originates not only from NH_4NO_3 decomposition (Reaction (11)) [42,43], but also from the direct reaction between NO_2 and adsorbed NH_3 (Reaction (13)) [44,45]. Reaction (13) also accounts for the NO_2 consumption at 250–375 °C in Fig. 5c. As NH_4NO_3 can also deposit on the catalysts in fast SCR condition [46], the NO consumption at 200–375 °C in Fig. 5b may be ascribed to the reaction between NO and NH_4NO_3 (Reaction (14)), which mitigates the NH_4NO_3 blockage effect and avoids N_2O release [43,47].



3.3. Reactions between HNCO and NO_x

To investigate the reactions between HNCO and NO_x , the urea-loaded catalysts were exposed to NO_x in the absence of H_2O vapor. The comparison between 2Cu-SAPO-34 (Fig. 6b) and SAPO-34 (Fig. S11a) suggests that pure SAPO-34 is almost inert for catalyzing HNCO-SCR of NO, while Cu species is necessary for HNCO conversion, as suggested by the significantly increased CO_2 release and NO_x conversion. Two NO_x reduction peaks can be observed in Fig. 6b, centered at 175 and 200 °C, respectively. The former one is also observed in TPSR curve of pre-adsorbed NH_3 with gaseous NO (Fig. S12), indicating that the main reducing agent participating in SCR at this stage is adsorbed NH_3 derived from urea thermolysis (Reaction (1)). At higher temperatures, HNCO also contributes directly to SCR (Reactions (5)–(7)), as implied by the remarkable CO_2 release. Table 5 shows that the catalysts with higher Cu loading and higher Cu dispersion converts more HNCO, indicating that isolated Cu^{2+} ions are the main active sites in this reaction.

The molar ratios of NH_3 to HNCO detected in the outlet gas suggest that NH_3 has higher reactivity than HNCO. In the absence of O_2 , the conversion of NH_3 is slightly higher than that of HNCO. It should be mentioned that HNCO hydrolysis (Reaction (2)) also contributes to the total HNCO conversion, as suggested by the CO_2 release peak below 150 °C like the case in urea thermolysis in N_2 (Fig. 2c). The presence of O_2 promotes the conversion of HNCO over 2Cu-SAPO-34, but the outlet NH_3/HNCO ratio decreases notably. Over 2Cu-SAPO-34 and 1Cu-SAPO-34, the molar ratios of the consumed N(-III) species to the reduced NO_x (calculated by Eq. (10)) is just slightly higher than 1, indicating that

most of NH_3 is consumed by NH_3 -SCR (Reaction (4)) rather than NH_3 oxidation. It can be inferred that NH_3 is a more active reducing agent than HNCO in SCR. More NH_3 is consumed over 1Cu-SAPO-34-i due to the stronger NH_3 oxidation activity of Cu_xO_y clusters [37,38,48,49].

When NO and NO_2 are fed in 1:1 ratio (Fig. 6c), the CO_2 concentration has already reached 100 ppm at 100 °C, suggesting that the reactivity of HNCO is promoted in this condition via Reaction (7) compared with the NO-only condition. Even so, the HNCO conversion (50%) is much lower than NH_3 conversion, as suggested by the remarkably decreased outlet NH_3/HNCO ratio. It can be inferred that HNCO-SCR is affected more severely than NH_3 -SCR by NH_4NO_3 deposition, as the NO over-consumption at around 250 °C reveals the formation of NH_4NO_3 (Reaction (14)). The onset temperature of HNCO release is significantly reduced, probably due to accelerated urea thermolysis by faster consumption of NH_3 . Fast SCR can also take place over pure SAPO-34 (Fig. S11b), with increased HNCO conversion and NH_3/HNCO ratio, implying that fast SCR of HNCO might be more favored over pure SAPO-34. However, the NO_x conversion is lower than that over 2Cu-SAPO-34, and a significant N_2O release with a maximum of 50 ppm is observed, due to the lack of active Cu species.

When NO_2 is fed solely (Fig. 6d), HNCO conversion suffers an almost thorough inhibition, while the conversion of NH_3 is less affected, as suggested by the lowest NH_3/HNCO ratio of 0.26. The over-consumption of the reducing agents is attributed to the oxidation of N(-III) to NO by NO_2 [8,10]. A large amount of N_2O is detected, indicating a serious NH_4NO_3 deposition, thus SCR is inhibited severely.

The in-situ DRIFT spectra of urea-impregnated 2Cu-SAPO-34 exposed to NO_x are shown in Fig. 7. In the presence of NO, both the band at 2264 cm^{-1} representing NCO^- adsorbed on SAPO-34 framework and the band at 2220 cm^{-1} representing Cu-NCO disappear at temperatures lower than in the absence of NO_x (Fig. 3d), indicating that HNCO can participate directly in SCR as a reducing agent when adsorbed on zeolite-based catalysts [36]. When NO_2 is present, the relative intensity of Cu-NCO band is lowered, especially in NO_2 only condition (Fig. 7c), probably because the active Cu sites are more easily blocked by NH_4NO_3 deposition, corresponding to the inhibited reactivity of HNCO in Fig. 6d.

4. Discussion

4.1. Active sites for urea-related reactions over Cu-SAPO-34

It is obvious that Cu species catalyze the thermolysis of urea and its by-products (Table 2). Larrubia et al. [27,28] have reported a detailed urea thermolysis mechanism that urea is first adsorbed as an anionic form on metal sites, and then is converted to adsorbed isocyanate anion and NH_3 molecule. M-NCO ($M = \text{Cu}, \text{Al}, \text{Si}$) species are found over SAPO-34 and Cu-SAPO-34 (Figs. 3 and S7) in the present work, coincide with the above-mentioned mechanism. To further study the behaviors of the M-NCO species under different conditions, the evolutions of their normalized band areas versus temperature are shown in Fig. 8. Over pure SAPO-34, the band at 2264 cm^{-1} (with a weak shoulder at 2215 cm^{-1}) representing NCO^- absorbed on the zeolite framework occurs at 125–150 °C. Besides the band at 2264 cm^{-1} , a distinct band at 2220 cm^{-1} representing Cu-NCO occurs over 2Cu-SAPO-34 at 100–125 °C, in accordance with the reduced onset temperature of urea thermolysis (Table 2). The normalized band area of Cu-NCO increases more quickly at temperatures lower than 200 °C, indicating that isolated Cu^{2+} ions are more active than the framework atoms for urea thermolysis at low temperatures. Another interesting observation is that the evolution of the 2264 cm^{-1} band over 2Cu-SAPO-34 is accelerated by the presence of Cu. This band occurs at lower temperatures over 2Cu-SAPO-34, and builds up more quickly than that over pure SAPO-34. This phenomenon can be assigned to the spillover effect of HNCO from Cu^{2+} ions to the SAPO-34 framework [35], further demonstrating the important role of Cu^{2+} ions in urea thermolysis.

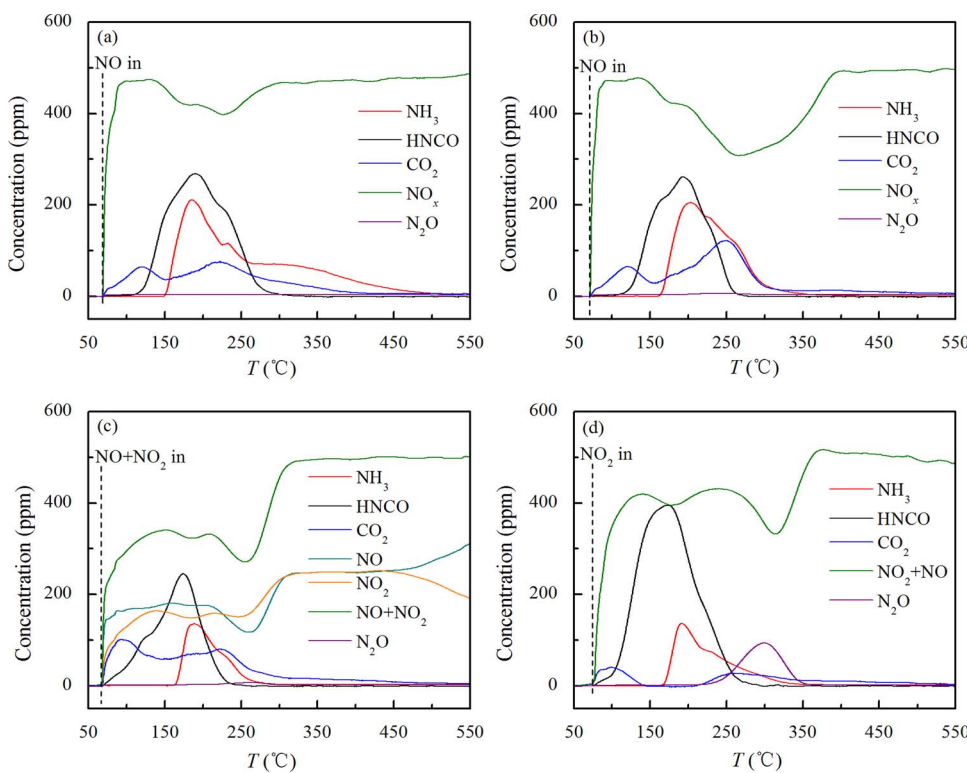


Fig. 6. Reactions of NO_x with urea over 2Cu-SAPO-34 in (a) 500 ppm NO/N₂, (b) 500 ppm NO/5% O₂/N₂, (c) 250 ppm NO/250 ppm NO₂/5% O₂/N₂ and (d) 500 ppm NO₂/5% O₂/N₂.

At temperatures higher than about 275 °C, the bands begin to decrease in intensity. Some stable M-NCO species still remain over the samples in N₂ (Fig. 8a), while the band intensities decrease drastically over 2Cu-SAPO-34 in the presence of O₂ (Fig. 8b). The vanished NCO⁻ species are oxidized to CO₂ catalyzed by Cu species (Fig. 2d). With the introduction of NO in Fig. 8c, the M-NCO species over 2Cu-SAPO-34 are eliminated at even lower temperatures. Again, the faster consumption of NCO⁻ by NO over 2Cu-SAPO-34 than over SAPO-34 indicates that Cu species catalyze HNCO-SCR. By comparison of the HNCO conversions over 2Cu-SAPO-34, 1Cu-SAPO-34 and 1Cu-SAPO-34-i (Table 5), it can be confirmed that isolated Cu²⁺ ions are the main active sites for this reaction, while Cu_xO_y clusters have inferior activity. In addition, a reverse spillover effect of NCO⁻ can be observed over 2Cu-SAPO-34. With increasing temperature, the band at 2264 cm⁻¹ over 2Cu-SAPO-34 diminishes more quickly than that over SAPO-34, and its evolution curve follows that of the 2220 cm⁻¹ band closely in the presence of both O₂ and NO + O₂. It is inferred that the NCO⁻ species adsorbed over the SAPO-34 framework can migrate back to Cu²⁺ ions and be consumed there at high temperatures. This reverse spillover effect gives further proof that isolated Cu²⁺ ions catalyze HNCO oxidation and HNCO-SCR. Pure SAPO-34 can also catalyze the reaction between adsorbed NCO⁻ and NO at high temperatures (Fig. 8c), but the HNCO conversion is quite low (Table 5).

It has been widely accepted that Ti-NCO is an intermediate for HNCO hydrolysis over anatase, and Lewis acid sites (coordinative unsaturated Ti⁴⁺) are active sites [23–26,29]. Besides, Piazzesi et al. [34] have concluded that Fe-NCO and Al-NCO on Fe-ZSM-5 can react with water to produce NH₃ and CO₂. Comparing the catalysts with similar Cu loadings, the HNCO hydrolysis activity follows the order of 1Cu-SAPO-34 > 1Cu-SAPO-34-i > 1CuO/SAPO-34-m (Table 3), in accordance with their band intensities of Cu-NCO (Fig. S7). Over the catalyst with a higher Cu dispersion, more unsaturated Cu²⁺ ions are available for HNCO adsorption and hydrolysis. Therefore, isolated Cu²⁺ ions are the most active copper species for HNCO hydrolysis. When increasing the Cu loading from 1 wt.% to 2 wt.%, the HNCO conversion increases slightly, probably due to more severe mass-transfer limitations with increased Cu loading [50].

In NH₃-SCR reaction, isolated Cu²⁺ ions have been proved to be the active sites over Cu-SAPO-34 catalysts [18,51–55]. Our study shows that isolated Cu²⁺ ions are also the most active sites in urea thermolysis, HNCO hydrolysis and HNCO-SCR, further illustrating the advantage of preparing Cu-SAPO-34 catalysts with isolated Cu²⁺ ions as the main Cu species when considering the potential NH₃ insufficiency at low temperatures.

Table 5
Results of the reactions between urea and NO_x over the catalysts.

Catalysts	Reaction conditions	HNCO conversion (%)	NH ₃ /HNCO detected	NO _x conversion (%)	Consumed N (–III) Reduced NO _x
SAPO-34	500 ppm NO/5% O ₂ /N ₂	18	1.05	< 5	–
SAPO-34	250 ppm NO/250 ppm NO ₂ /5% O ₂ /N ₂	56	0.89	12	1.04
1Cu-SAPO-34	500 ppm NO/5% O ₂ /N ₂	33	0.82	13	1.04
1Cu-SAPO-34-i	500 ppm NO/5% O ₂ /N ₂	31	0.79	12	1.23
2Cu-SAPO-34	500 ppm NO/N ₂	25	0.95	< 5	–
2Cu-SAPO-34	500 ppm NO/5% O ₂ /N ₂	38	0.83	14	1.04
2Cu-SAPO-34	250 ppm NO/250 ppm NO ₂ /5% O ₂ /N ₂	50	0.47	17	1.02
2Cu-SAPO-34	500 ppm NO ₂ /5% O ₂ /N ₂	13	0.26	6	1.43

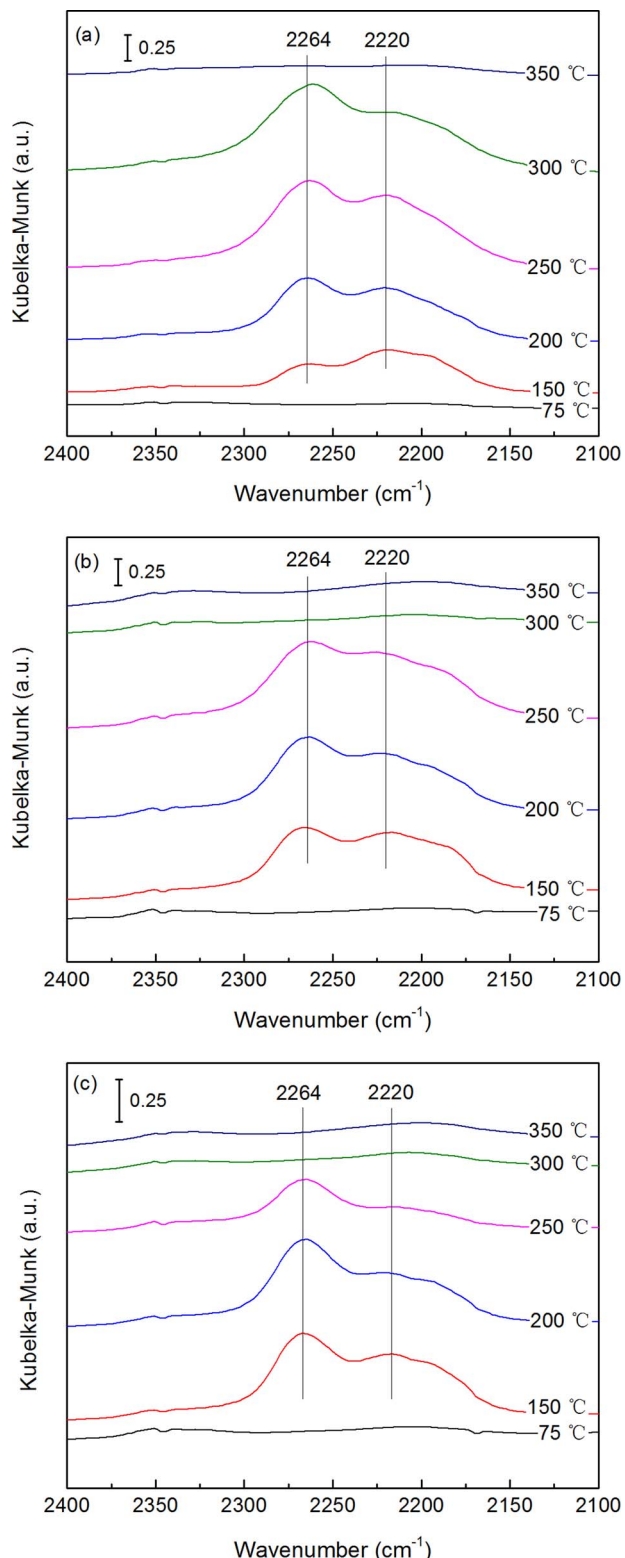


Fig. 7. In-situ DRIFT spectra of the reactions between urea and NO_x over 2Cu-SAPO-34 in (a) 500 ppm NO/5% O₂/N₂, (b) 250 ppm NO/250 ppm NO₂/5% O₂/N₂ and (c) 500 ppm NO₂/5% O₂/N₂.

4.2. Role of HNCO in urea-SCR

HNCO is an important intermediate in urea-related reactions and is usually regarded as an ammonia precursor. Meanwhile, HNCO can also act directly as a reducing agent over Cu-SAPO-34 (Table 5). The

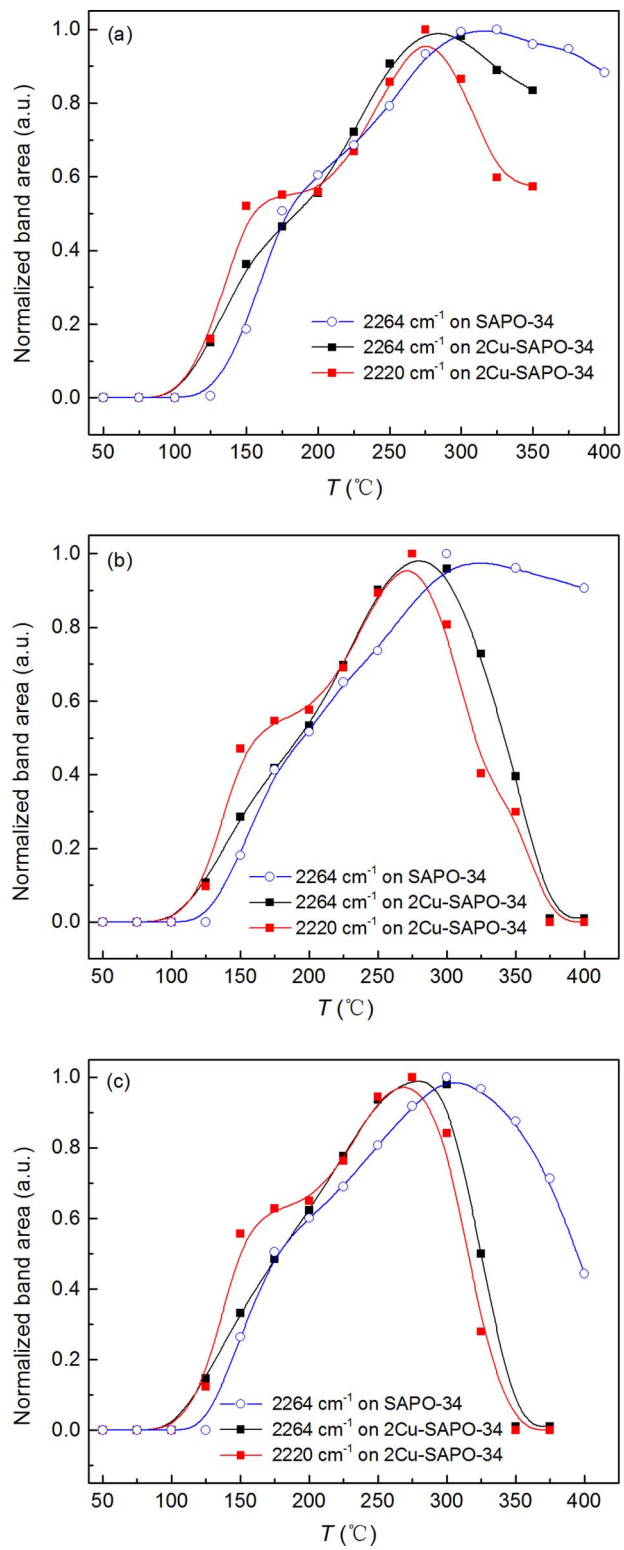
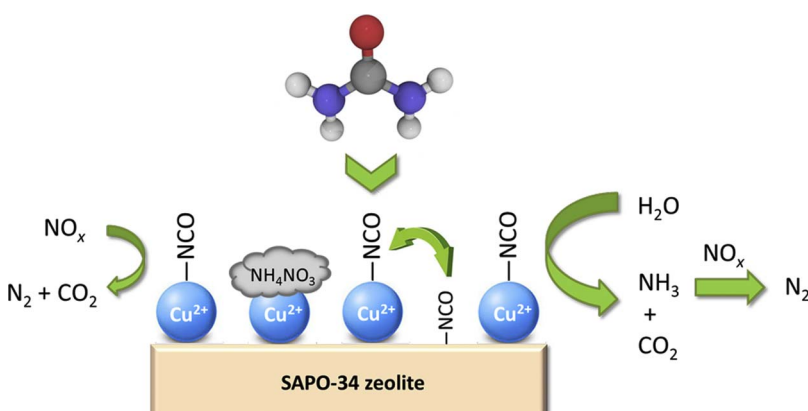
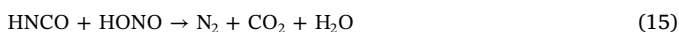


Fig. 8. Evolution of normalized band areas of HNCO-related species versus temperature over SAPO-34 and 2Cu-SAPO-34 in (a) N₂, (b) 5% O₂/N₂ and (c) 500 ppm NO/5% O₂/N₂.

reaction between HNCO and NO in the absence of O₂ is observed over Cu-SAPO-34, and the presence of O₂ further improves the HNCO conversion. Based on the stoichiometric ratios between N(III) species and NO_x (Table 5), Reaction (6) can be determined to be the main reaction in HNCO-SCR over Cu-SAPO-34 catalysts. Seneque et al. [10] have reported that the presence of NO₂ significantly improves the reactivity of HNCO via forming HONO intermediate (Reaction (15)). The total



reaction can be written as Reaction (7), similar to fast SCR between NH₃ and NO_x (Reaction (8)). Reaction (7) is also observed over Cu-SAPO-34 in the present work, giving higher HNCO and NO_x conversions than in the absence of NO₂. It can be inferred that the presence of O₂ promotes the reaction between NO and HNCO via producing active intermediates such as NO₂, nitrates and nitrites [56–59]. Another possible explanation is that O₂ contributes to the oxidation of Cu⁺ to Cu²⁺ to fulfill the redox cycle of Cu in SCR [60–62]. HNCO can also be oxidized by O₂ at high temperatures (Reaction (16)) [8,36]. The reaction network is quite complicated in urea-SCR, so the stoichiometry and detailed mechanism of HNCO-SCR wait to be further investigated.



By comparing the conversions of HNCO and NH₃ with NO_x (Table 5), it can be seen that NH₃ is a more active reducing agent in SCR over Cu-SAPO-34 catalysts. Moreover, the HNCO conversion in urea hydrolysis (Figs. 4c and 5a) is significantly higher than that in HNCO-SCR of NO (Fig. 6b). This, as well as the fact that HNCO hydrolysis finishes at lower temperatures, indicates that the former reaction is faster than HNCO-SCR. In the presence of NO₂, the reactivity of HNCO as a reducing agent is promoted over Cu-SAPO-34 catalysts via fast SCR (Reaction (7)). However, NH₄NO₃ deposition due to the introduction of NO₂ (Reaction (12)) may inhibit both SCR [63] and HNCO hydrolysis [29] at low temperatures. Comparing the conversions of HNCO and NH₃ in the presence of NO₂ (Fig. 6c and d), it can be inferred that HNCO-SCR is more susceptible to NH₄NO₃ deposition than NH₃-SCR. Besides, the HNCO conversion is much higher in the presence of H₂O (Fig. 5b and c) than without H₂O (Fig. 6c and d). These observations demonstrate the importance of HNCO hydrolysis in urea-SCR, even in fast SCR condition. Seker et al. [11] reported that NO_x conversion over a Pt/Al₂O₃ catalyst significantly decreased with decreasing H₂O concentration due to insufficient NH₃ supply, but the promotion effect of H₂O is not pronounced in this work. This discrepancy might be explained by excess NH₃ supply originated from the thermolysis of pre-impregnated urea at temperatures lower than 250 °C in our test (Fig. 6b). The excess NH₃ supply compensates the inferior reactivity of HNCO in SCR and covers up the problem of NH₃ insufficiency when HNCO hydrolysis scarcely takes place. In fact, in more realistic test conditions, incomplete HNCO hydrolysis leads to a remarkably increased slip of unreacted reducing agents, especially HNCO, while NH₃ originated from urea and HNCO can be adsorbed and utilized at downstream of catalyst monolith [12]. Based on the above argument, it can be concluded that in urea-SCR over Cu-SAPO-34, the main reaction pathway of HNCO is being hydrolyzed to NH₃ prior to participating in SCR at temperatures below 250 °C. The inferred reaction pathways of HNCO are summarized in Fig. 9. However, our experiment method did not allow us to study the behaviors of urea and HNCO at higher temperatures and with continuous feeding of urea and HNCO, so detailed

Fig. 9. Schematic of the reaction pathways of HNCO in urea-SCR over Cu-SAPO-34 at low temperatures.

studies under more realistic conditions are required to understand the role of HNCO in urea-SCR comprehensively.

5. Conclusions

In this work, a series of Cu-SAPO-34 catalysts with different Cu species and Cu loadings were prepared to study the urea-related reactions and identify their active sites. Cu-SAPO-34 catalysts prepared by the ion-exchange method have the highest activity for urea thermolysis and hydrolysis, especially at low temperatures. The onset temperatures of urea thermolysis and hydrolysis are both reduced by about 30 °C over Cu-SAPO-34 catalysts compared with pure SAPO-34. In the simulative urea hydrolysis test with 10 wt.% pre-impregnated urea, Cu-SAPO-34 catalysts convert more than 85% of urea to NH₃ and CO₂. Cu-SAPO-34 catalysts also catalyze HNCO-SCR, converting more than 30% of HNCO via the reaction between HNCO and NO_x under the simulative test conditions. Isolated Cu²⁺ ions are identified as the main active sites for these reactions.

In urea-SCR, NH₃ formed via urea thermolysis and hydrolysis is the main reducing agent at temperatures lower than 250 °C. HNCO is less active than NH₃ to react with NO and acts mainly as an ammonia precursor. HNCO hydrolysis is scarcely affected by NO at temperatures lower than 250 °C, but is severely inhibited by NH₄NO₃ deposition in the presence of NO₂. HNCO-SCR is promoted in fast SCR condition, but suffers more severe inhibition from NH₄NO₃ deposition than NH₃-SCR.

Based on these findings, suggestions can be given that Cu-SAPO-34 catalysts with isolated Cu²⁺ ions as the main Cu species are required for urea-SCR when considering the potential insufficient supply of reducing agents at low temperatures, and the NO₂/NO_x ratio should be carefully optimized to improve the deNO_x efficiency of urea-SCR systems in diesel vehicles.

Acknowledgements

The authors would like to acknowledge the financial support from projects of China Science and Technology Exchange Center (No. 2016YFE0126600), the National Key R&D Program of China (Nos. 2017YFC0211102 and 2017YFC0211202).

Appendix A. Supplementary data

Supplementary data associated with this article can be found, in the online version, at <https://doi.org/10.1016/j.apcatb.2018.01.026>.

References

- [1] S.D. Yim, S.J. Kim, J.H. Baik, I.S. Nam, Y.S. Mok, J. Lee, B.K. Cho, S.H. Oh, Ind. Eng. Chem. Res. 43 (2004) 4856–4863.
- [2] S. Selandius, T.T. Le, L.J. Pettersson, H. Lind, Chem. Eng. J. 231 (2013) 220–226.
- [3] V. Ebrahimian, A. Nicolle, C. Habchi, AIChE J. 58 (2012) 1998–2009.

- [4] H.L. Fang, H.F.M. DaCosta, *Appl. Catal. B: Environ.* 46 (2003) 17–34.
- [5] A. Lundström, B. Andersson, L. Olsson, *Chem. Eng. J.* 150 (2009) 544–550.
- [6] E. Abu-Ramadan, K. Saha, X. Li, *AIChE J.* 57 (2011) 3210–3225.
- [7] M. Koebel, M. Elsener, *J. Chromatogr. A* 689 (1995) 164–169.
- [8] M. Seneque, F. Can, D. Duprez, X. Courtois, *Catalysts* 5 (2015) 1535–1553.
- [9] M. Koebel, M. Elsener, T. Marti, *Combust. Sci. Technol.* 121 (1996) 85–102.
- [10] M. Seneque, F. Can, D. Duprez, X. Courtois, *ACS Catal.* 6 (2016) 4064–4067.
- [11] E. Seker, N. Yasyerli, E. Gulari, C. Lambert, R.H. Hammerle, *Appl. Catal. B: Environ.* 37 (2002) 27–35.
- [12] M. Kleemann, M. Elsener, M. Koebel, A. Wokaun, *Ind. Eng. Chem. Res.* 39 (2000) 4120–4126.
- [13] L. Xu, W. Watkins, R. Snow, G. Graham, R. McCabe, C. Lambert, R.O. Carter, *SAE 2007* (2007) 01–1582.
- [14] M. Eichelbaum, A.B. Siemer, R.J. Farrauto, M.J. Castaldi, *Appl. Catal. B: Environ.* 97 (2010) 98–107.
- [15] A.M. Bernhard, D. Peitz, M. Elsener, A. Wokaun, O. Kröcher, *Appl. Catal. B: Environ.* 115–116 (2012) 129–137.
- [16] G. Cavataio, J. Girard, J.E. Patterson, C. Montreuil, Y. Cheng, C.K. Lambert, *SAE 2007* (2007) 01–1575.
- [17] D.W. Fickel, E.D. Addio, J.A. Lauterbach, R.F. Lobo, *Appl. Catal. B: Environ.* 102 (2011) 441–448.
- [18] J. Wang, H. Zhao, G. Haller, Y. Li, *Appl. Catal. B: Environ.* 202 (2017) 346–354.
- [19] J.H. Lee, Y.J. Kim, T. Ryu, P.S. Kim, C.H. Kim, S.B. Hong, *Appl. Catal. B: Environ.* 200 (2017) 428–438.
- [20] U. De-La-Torre, B. Pereda-Ayo, M. Moliner, J.R. González-Velasco, A. Corma, *Appl. Catal. B: Environ.* 187 (2016) 419–427.
- [21] A. Lundström, T. Snelling, P. Morsing, P. Gabrielsson, E. Senar, L. Olsson, *Appl. Catal. B: Environ.* 106 (2011) 273–279.
- [22] A.M. Bernhard, D. Peitz, M. Elsener, T. Schildhauer, O. Kröcher, *Catal. Sci. Technol.* 3 (2013) 942–951.
- [23] G. Piazzesi, O. Kröcher, M. Elsener, A. Wokaun, *Appl. Catal. B: Environ.* 65 (2006) 55–61.
- [24] I. Czekaj, O. Kröcher, G. Piazzesi, *J. Mol. Catal. A: Chem.* 280 (2008) 68–80.
- [25] P. Hauck, A. Jentys, J.A. Lercher, *Catal. Today* 127 (2007) 165–175.
- [26] P. Hauck, A. Jentys, J.A. Lercher, *Appl. Catal. B: Environ.* 70 (2007) 91–99.
- [27] M.A. Larrubia, G. Ramis, G. Busca, *Appl. Catal. B: Environ.* 30 (2001) 101–110.
- [28] M.A. Larrubia, G. Ramis, G. Busca, *Appl. Catal. B: Environ.* 27 (2000) L145–L151.
- [29] G. Piazzesi, M. Elsener, O. Kröcher, A. Wokaun, *Appl. Catal. B: Environ.* 65 (2006) 169–174.
- [30] M. Goldbach, A. Roppertz, P. Langenfeld, M. Wackerhagen, S. Füger, S. Kureti, *Chem. Eng. Technol.* 40 (2017) 2035–2043.
- [31] Y. Wang, X. Zhu, Y. Huang, C. Zheng, X. Gao, *RSC Adv.* 6 (2016) 108000–108009.
- [32] A.M. Bernhard, I. Czekaj, M. Elsener, O. Kröcher, *Appl. Catal. B: Environ.* 134–135 (2013) 316–323.
- [33] M. Eichelbaum, R.J. Farrauto, M.J. Castaldi, *Appl. Catal. B: Environ.* 97 (2010) 90–97.
- [34] G. Piazzesi, D. Nicosia, M. Devadas, O. Kröcher, M. Elsener, A. Wokaun, *Catal. Lett.* 115 (2007) 33–39.
- [35] F. Solymosi, T. Bansagi, *J. Catal.* 156 (1995) 75–84.
- [36] H. Takeda, M. Iwamoto, *Catal. Lett.* 38 (1996) 21–25.
- [37] X. Liu, X. Wu, D. Weng, Z. Si, R. Ran, *Catal. Today* 281 (2016) 596–604.
- [38] J. Wang, Y. Huang, T. Yu, S. Zhu, M. Shen, W. Li, J. Wang, *Catal. Sci. Technol.* 4 (2014) 3004.
- [39] P.M. Schaber, J. Colson, S. Higgins, D. Thielen, B. Anspach, J. Brauer, *Thermochim. Acta* 424 (2004) 131–142.
- [40] O. Mihai, C.R. Widjastuti, S. Andonova, K. Kamasamudram, J. Li, S.Y. Joshi, N.W. Currier, A. Yezerets, L. Olsson, *J. Catal.* 311 (2014) 170–181.
- [41] Z. Chen, Z. Si, L. Cao, X. Wu, R. Ran, D. Weng, *Catal. Sci. Technol.* 7 (2017) 2531–2541.
- [42] H. Chen, Z. Wei, M. Kollar, F. Gao, Y. Wang, J. Szanyi, C.H.F. Peden, *J. Catal.* 329 (2015) 490–498.
- [43] A. Grossale, I. Nova, E. Tronconi, *J. Catal.* 265 (2009) 141–147.
- [44] H. Zhu, J.H. Kwak, C.H.F. Peden, J. Szanyi, *Catal. Today* 205 (2013) 16–23.
- [45] A. Grossale, I. Nova, E. Tronconi, D. Chatterjee, M. Weibel, *Top. Catal.* 52 (2009) 1837–1841.
- [46] K. Leistner, O. Mihai, K. Wijayant, A. Kumar, K. Kamasamudram, N.W. Currier, A. Yezerets, L. Olsson, *Catal. Today* 258 (2015) 49–55.
- [47] W. Su, H. Chang, Y. Peng, C. Zhang, J. Li, *Environ. Sci. Technol.* 49 (2015) 467–473.
- [48] Y. Jangjou, M. Ali, Q. Chang, D. Wang, J. Li, A. Kumar, W.S. Epling, *Catal. Sci. Technol.* 6 (2016) 2679–2685.
- [49] Z. Zhao, R. Yu, R. Zhao, C. Shi, H. Gies, F. Xiao, D. De Vos, T. Yokoi, X. Bao, U. Kolb, M. Feyen, R. McGuire, S. Maurer, A. Moini, U. Müller, W. Zhang, *Appl. Catal. B: Environ.* 217 (2017) 421–428.
- [50] F. Gao, E.D. Walter, E.M. Karp, J. Luo, R.G. Tonkyn, J.H. Kwak, J. Szanyi, C.H.F. Peden, *J. Catal.* 300 (2013) 20–29.
- [51] J. Xue, X. Wang, G. Qi, J. Wang, M. Shen, W. Li, *J. Catal.* 297 (2013) 56–64.
- [52] L. Wang, W. Li, G. Qi, D. Weng, *J. Catal.* 289 (2012) 21–29.
- [53] S.A. Bates, A.A. Verma, C. Paolucci, A.A. Parekh, T. Anggara, A. Yezerets, W.F. Schneider, J.T. Miller, W.N. Delgass, F.H. Ribeiro, *J. Catal.* 312 (2014) 87–97.
- [54] A.M. Beale, F. Gao, I. Lezcano-Gonzalez, C.H.F. Peden, J. Szanyi, *Chem. Soc. Rev.* 44 (2015) 7371–7405.
- [55] S.T. Korhonen, D.W. Fickel, R.F. Lobo, B.M. Weckhuysen, A.M. Beale, *Chem. Commun.* 47 (2011) 800–802.
- [56] M.P. Ruggeri, T. Selleri, M. Colombo, I. Nova, E. Tronconi, *J. Catal.* 311 (2014) 266–270.
- [57] L. Ma, Y. Cheng, G. Cavataio, R.W. McCabe, L. Fu, J. Li, *Appl. Catal. B: Environ.* 156–157 (2014) 428–437.
- [58] D. Wang, L. Zhang, K. Kamasamudram, W.S. Epling, *ACS Catal.* 3 (2013) 871–881.
- [59] M.P. Ruggeri, I. Nova, E. Tronconi, J.A. Pihl, T.J. Toops, W.P. Partridge, *Appl. Catal. B: Environ.* 166–167 (2015) 181–192.
- [60] T. Günter, H.W.P. Carvalho, D.E. Doronkin, T. Sheppard, P. Glatzel, A.J. Atkins, J. Rudolph, C.R. Jacob, M. Casapu, J. Grunwaldt, *Chem. Commun.* 51 (2015) 9227–9230.
- [61] C. Paolucci, A.A. Verma, S.A. Bates, V.F. Kispersky, J.T. Miller, R. Gounder, W.N. Delgass, F.H. Ribeiro, W.F. Schneider, *Angew. Chem. Int. Ed.* 53 (2014) 11828–11833.
- [62] C. Paolucci, I. Khurana, A.A. Parekh, S. Li, A.J. Shih, H. Li, J.R. Di Iorio, J.D. Albaracin-Caballero, A. Yezerets, J.T. Miller, W.N. Delgass, F.H. Ribeiro, W.F. Schneider, R. Gounder, *Science* 357 (2017) 898–903.
- [63] L. Xie, F. Liu, K. Liu, X. Shi, H. He, *Catal. Sci. Technol.* 4 (2014) 1104.